CellPress
PARTNER JOURNAL

Molecular Plant
Research Article

Translational Regulation of Metabolic Dynamics during Effector-Triggered Immunity

Heejin Yoo[1,3,7], George H. Greene[1,7], Meng Yuan[2,7], Guoyong Xu[1,4], Derek Burton[1], Lijing Liu[1,5], Jorge Marqués[1,6] and Xinnian Dong[1,*]

[1]Howard Hughes Medical Institute, Department of Biology, Duke University, Box 90338, Durham, NC 27708, USA

[2]National Key Laboratory of Crop Genetic Improvement, National Centre of Plant Gene Research (Wuhan), Huazhong Agricultural University, 430070 Wuhan, China

[3]Present address: Department of Plant Biology, Ecology, and Evolution, Oklahoma State University, Stillwater, OK 74078, USA

[4]Present address: National Key Laboratory of Hybrid Rice, Institute for Advanced Studies (IAS), Wuhan University, Wuhan, Hubei 430072, China

[5]Present address: Key Laboratory of Plant Development and Environment Adaptation Biology, Ministry of Education, School of Life Sciences, Shandong University, Qingdao, China

[6]Present address: David H. Murdock Research Institute, Kannapolis, NC 28081, USA

[7]These authors contributed equally in this article.

***Correspondence: Xinnian Dong (xdong@duke.edu)**

https://doi.org/10.1016/j.molp.2019.09.009

ABSTRACT

Recent studies have shown that global translational reprogramming is an early activation event in pattern-triggered immunity, when plants recognize microbe-associated molecular patterns. However, it is not fully known whether translational regulation also occurs in subsequent immune responses, such as effector-triggered immunity (ETI). In this study, we performed genome-wide ribosome profiling in *Arabidopsis* upon RPS2-mediated ETI activation and discovered that specific groups of genes were translationally regulated, mostly in coordination with transcription. These genes encode enzymes involved in aromatic amino acid, phenylpropanoid, camalexin, and sphingolipid metabolism. The functional significance of these components in ETI was confirmed by genetic and biochemical analyses. Our findings provide new insights into diverse translational regulation of plant immune responses and demonstrate that translational coordination of metabolic gene expression is an important strategy for ETI.

Key words: translational regulation, ribosome profiling, effector-triggered immunity, ETI, phenylalanine, phenylpropanoids, helper receptors

Yoo H., Greene G.H., Yuan M., Xu G., Burton D., Liu L., Marqués J., and Dong X. (2020). Translational Regulation of Metabolic Dynamics during Effector-Triggered Immunity. Mol. Plant. **13**, 88–98.

INTRODUCTION

With the recent application of high-throughput sequencing to ribosome footprinting (Ribo-seq), translational reprogramming has been found to play a significant role in plant responses to various environmental stimuli including pathogens, light, hypoxia, drought, ethylene, and heat stress (Liu et al., 2013; Yángüez et al., 2013; Juntawong et al., 2014; Lei et al., 2015; Merchante et al., 2015; Xu et al., 2017a; Meteignier et al., 2017). Ribo-seq analysis of pattern-triggered immunity (PTI), the first layer of active immune response to microbe-associated molecular patterns, showed that translational reprogramming occurs early in this immune response, most likely before the major transcriptional event (Xu et al., 2017a). However, it is not fully understood how translational regulation is involved in subsequent immune responses, including effector-triggered immunity (ETI), which is induced through recognition of pathogen effectors by the host nucleotide binding site and leucine-rich repeat (NBS–LRR) domain containing immune receptors; for example, AvrRpm1 and AvrRpt2 effectors are recognized by RPM1 and RPS2, respectively, to confer resistance (Grant et al., 1995; Mindrinos et al., 1994). Recently, a translational response to the pathogen effector, AvrRpm1, expressed in *Arabidopsis* as a transgene was reported (Meteignier et al., 2017). This study showed that recognition of AvrRpm1 through RPM1 could influence the translational status of thousands of transcripts, including the stress-responsive translational regulator target of rapamycin kinase. However, fundamental questions still remain to be answered. Since ETI is the ultimate immune response because it often leads to the programmed cell death (PCD), is it possible that ETI-mediated PCD involves a global translation shutdown? Is global translational regulation distinct between PTI and ETI?

Published by the Molecular Plant Shanghai Editorial Office in association with Cell Press, an imprint of Elsevier Inc., on behalf of CSPB and IPPE, CAS.

Are the targets of translational regulation during ETI specific or similar for different immune receptors?

To answer these fundamental questions, we performed a global translatome analysis of the response to the bacterial pathogen *Pseudomonas syringae* pv. *maculicola* (*Psm*) ES4326 carrying the effector gene *AvrRpt2* (*Psm* ES4326/*AvrRpt2*) using the Ribo-seq strategy (Ingolia et al., 2009; Xu et al., 2017a). We discovered a targeted translational response in coordination with transcriptional regulation in a subset of genes involved in effector perception/signaling and several metabolic pathways. We further demonstrated genetically that these metabolic genes are specifically important for immune response during ETI. Together, our study provides new insights into translational regulation during ETI, which link metabolic dynamics to the immune response in plants.

RESULTS

ETI-Induced TBF1 Translation Occurs Later than PTI-Induced Translation

To determine the optimal condition for the global translatome analysis, we used the constitutively transcribed *35S:uORFs$_{TBF1}$-LUC* reporter in wild type (WT) and as a control, the NBS–LRR receptor mutant *rps2*, which fails to recognize the AvrRpt2 effector (Mindrinos et al., 1994) (Figure 1A). Translation of the luciferase reporter is controlled by the upstream open reading frames (uORFs) of the immune transcription factor gene *TBF1* (*uORFs$_{TBF1}$*), which has been shown to be rapidly induced by multiple pathogenic signals (Xu et al., 2017b). We found a dramatic induction of the luciferase activity by *Psm* ES4326/*AvrRpt2* between 6 and 8 h post infiltration (hpi) in WT, while no significant changes were detected in the *rps2* mutant (Figure 1B), indicating that the observed translational change in the reporter was dependent on the RPS2 receptor. Consistent with the induction of the luciferase reporter, the endogenous *TBF1* mRNA was enriched in polysome-associated fractions at 8 hpi in response to *Psm* ES4326/*AvrRpt2* (Figure 1C). In contrast to WT, the *rps2* mutant failed to increase translation of the endogenous *TBF1* mRNA (Figure 1D and 1E).

Notably, ETI-induced TBF1 translation occurred later than the PTI-induced translation induction (Xu et al., 2017a). Moreover, we did not detect a significant difference between the overall polysome profiles of mock-treated or *Psm* ES4326/*AvrRpt2*-inoculated samples collected at 8 hpi (Figure 1D), suggesting that, instead of a global shutdown of translation, ETI may involve targeted changes in active translation, including induction of TBF1 translation (Figure 1E).

Global Translatome Analysis Reveals Distinct Translational Regulation during ETI in Coordination with Transcriptional Regulation

To identify genes that undergo targeted changes in active translation during ETI, we collected *Arabidopsis* leaves at 8 h after either mock or *Psm* ES4326/*AvrRpt2* infection (OD_{600nm} = 0.02) and generated libraries for RNA sequencing (RNA-seq [RS]) and Ribo-seq (RF) analyses. The library construction and quality control are detailed in the Methods (Supplemental Figures 1 and 2). We compared the *Psm* ES4326/*AvrRpt2*-inoculated samples versus mock-inoculated samples and found 983 and 203 genes transcriptionally upregulated (RSup) and downregulated (RSdn), respectively, in WT plants (Supplemental Data 1). Differential analysis of RF fold change (RFfc) detected 926 genes with increased ribosome occupancy (RFup) and 156 genes with decreased ribosome occupancy (RFdn) (Supplemental Table 1). In the *rps2* mutant, only a small number of genes responded differentially in RS (20 RSup and 21 RSdn) and RF (15 RFup and six RFdn) (Supplemental Data 2 and Supplemental Figure 2H). Considering that similar observations were made in a previous microarray experiment with the same *Psm* ES4326/*AvrRpt2* (Gu et al., 2016) and a previous RNA-seq experiment with *Pseudomonas syringae* pv. *tomato* carrying the effector gene *AvrRpt2* (Mine et al., 2018), the small RS and RF changes in the *rps2* mutant were attributable to the specific sampling time used in this analysis.

Interestingly, in contrast to the poor correlation between transcriptional and translational changes during PTI (r = 0.41) (Xu et al., 2017a), changes in transcription and translation during ETI showed a relatively strong correlation (r = 0.92; Figure 2A), indicating that most translational changes during ETI were coordinated with changes in transcription. Nevertheless, in combination with transcriptional induction, significant translational induction is detected for the *TBF1* transcript in WT (Supplemental Figure 3A), implying that translational regulation indeed occurs during ETI. To identify translationally regulated genes during ETI, we calculated translational efficiency (TE) according to the previously reported formula (Ingolia et al., 2009; Xu et al., 2017a) and identified 594 mRNAs showing increased TE fold change (TEfc) and 523 mRNAs displaying decreased TEfc ($|z| \geq 1.5$) (Figure 2B and Supplemental Figure 3B and Supplemental Data 1). We performed dispersion analysis to filter out genes with small changes in RS and RF and found 157 mRNAs showing increased TE and 109 mRNAs showing decreased TE (Supplemental Figure 1H).

Identification of Translationally Responsive Regulators of ETI

For genetic analysis of potential novel regulators of ETI, we included the top TEup (TU) or TEdn (TD) genes based on our TE (Figure 2B) and dispersion analyses (Supplemental Figure 1H). We further extended our candidates (EC) from TE changed genes to include those with RFup changes such as genes encoding Toll interleukin-1 receptor nucleotide binding site domain (TIR–NBS), leucine-rich repeat domain (LRR), and TIR–NBS–LRR domain-containing proteins and proteins involved in sphingolipid metabolism, which were implicated in ETI in previous studies (Aboul-Soud et al., 2009; Padmanabhan et al., 2009; Swiderski et al., 2009; Zhang et al., 2010; Berkey et al., 2012; Nandety et al., 2013; Sánchez-Rangel et al., 2015). Using these selection criteria, we identified 50 candidate genes (27 TU, 11 TD, and 12 EC) (Supplemental Data 3; Figure 2B and Supplemental Figure 1H).

We obtained available T-DNA insertional mutants for 26 of these genes (11 TU, 6 TD, and 9 EC) and tested them for *Psm* ES4326/*AvrRpt2*-mediated ETI resistance by measuring both *in planta* bacterial growth as well as ion leakage resulting from PCD (Supplemental Data 3). Through these measurements, we

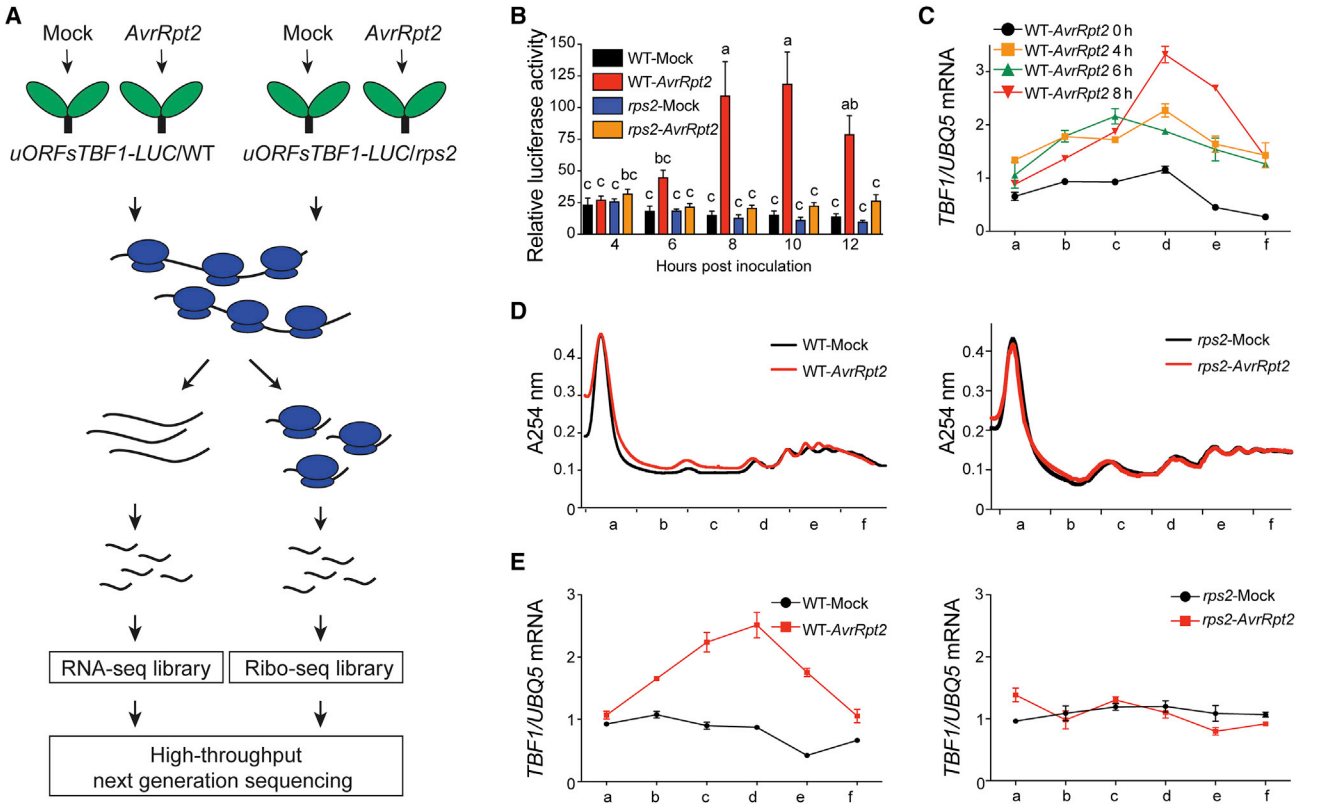

Figure 1. Translational Activities during ETI.

(A) Schematic of RNA-seq and Ribo-seq (RF) library construction using *35S:uORFs$_{TBF1}$-LUC*/WT and *35S:uORFs$_{TBF1}$-LUC/rps2* plants.

(B) Translation of the *35S:uORFs$_{TBF1}$-LUC* reporter in wild type (WT) and the *rps2* mutant after Mock (10 mM $MgCl_2$) or *Psm* ES4326/*AvrRpt2* (AvrRpt2) treatment (OD_{600nm} = 0.02). Relative LUC activity was normalized to the level at 1 h post infiltration (hpi). Data are means ± SEM; *n* = 6 biological replicates. Error bars with different letters represent statistically significant differences based on Tukey's test ($P < 0.05$; one-way ANOVA).

(C) *TBF1* mRNA associated with polysomal fractions at different time points after *Psm* ES4326/*AvrRpt2* treatment (OD_{600nm} = 0.02) (means ± SD; *n* = 4 technical replicates from one representative experiment). *TBF1 mRNA* abundance was normalized to the level of *UBQ5* mRNA in all fractions. Lower-case letters in the x axis indicate polysomal fractions in the polysome profile obtained by sucrose density gradient fractionation.

(D and E) Polysome profiling of global translational activity at 8 hpi **(D)** and *TBF1* mRNA translational activity **(E)** calculated as ratios of polysomal/total mRNA in WT (left panel) and *rps2* (right panel) after *Psm* ES4326/*AvrRpt2* treatment (OD_{600nm} = 0.02). Transcript levels of *TBF1* were normalized against *UBQ5* levels determined by qRT–PCR and ratios of polysomal fractions over the total mRNA are presented. Data are means ± SD; *n* = 4 technical replicates.

found 15 mutants compromised in at least one of these two phenotypes (Figure 2C–2E and Supplemental Table 1). It is worth noting that the defects detected in these mutants were ETI specific, because the mutants displayed similar growth of the isogenic *Psm* ES4326 lacking the AvrRpt2 effector as WT (Figure 2C–2E, left panels). Based on the patterns of *Psm* ES4326/*AvrRpt2* growth and ion leakage analysis, the ETI mutants can be further categorized into three distinct groups. Group A showed reduced PCD, accompanied with increased *Psm* ES4326/*AvrRpt2* bacterial growth compared with WT (Figure 2C). This is a typical mutant phenotype for a positive regulator of ETI. The nine genes in this group include inositol phosphorylceramide (a sphingolipid) synthase 2, the abscisic acid receptor PYL1, TIR–NBS–LRR, TIR–NBS, and LRR proteins, amino acid permease 3, and a chaperone DnaJ-domain protein. Group B mutants showed more *Psm* ES4326/*AvrRpt2* bacterial growth, but WT levels of ion leakage (Figure 2D). The three mutants in group B represent genes encoding two transporters (one for transporting histidine and lysine, and the other for a golgi nucleotide sugar transporter important for sphingolipid metabolism), and one TIR–NBS–LRR immune receptor. Group C mutants showed reduced ion leakage upon *Psm* ES4326/*AvrRpt2* treatment, but without a detectable increase in *Psm* ES4326/*AvrRpt2* pathogen growth compared with WT (Figure 2E). Genes represented by group C mutants may have a more significant role in ETI-associated PCD than restricting pathogen growth (Coll et al., 2010). They included a phosphate transporter, one enzyme in photorespiration, and a D111/G-patch domain-containing protein which may be involved in RNA binding and processing based on functional studies of its homologs (Aravind and Koonin, 1999).

To further confirm that these ETI-regulated genes are indeed translationally regulated, we performed ribosome pelleting experiments. We found that most of these candidate mRNAs displayed a consistent change with the Ribo-seq result in their association with the ribosome upon ETI induction, suggesting a contribution of translational regulation to their expression (Figure 3). Only three mRNAs, EC6, EC8, and TD2, did not recapitulate the Ribo-seq dynamics, probably due to differences

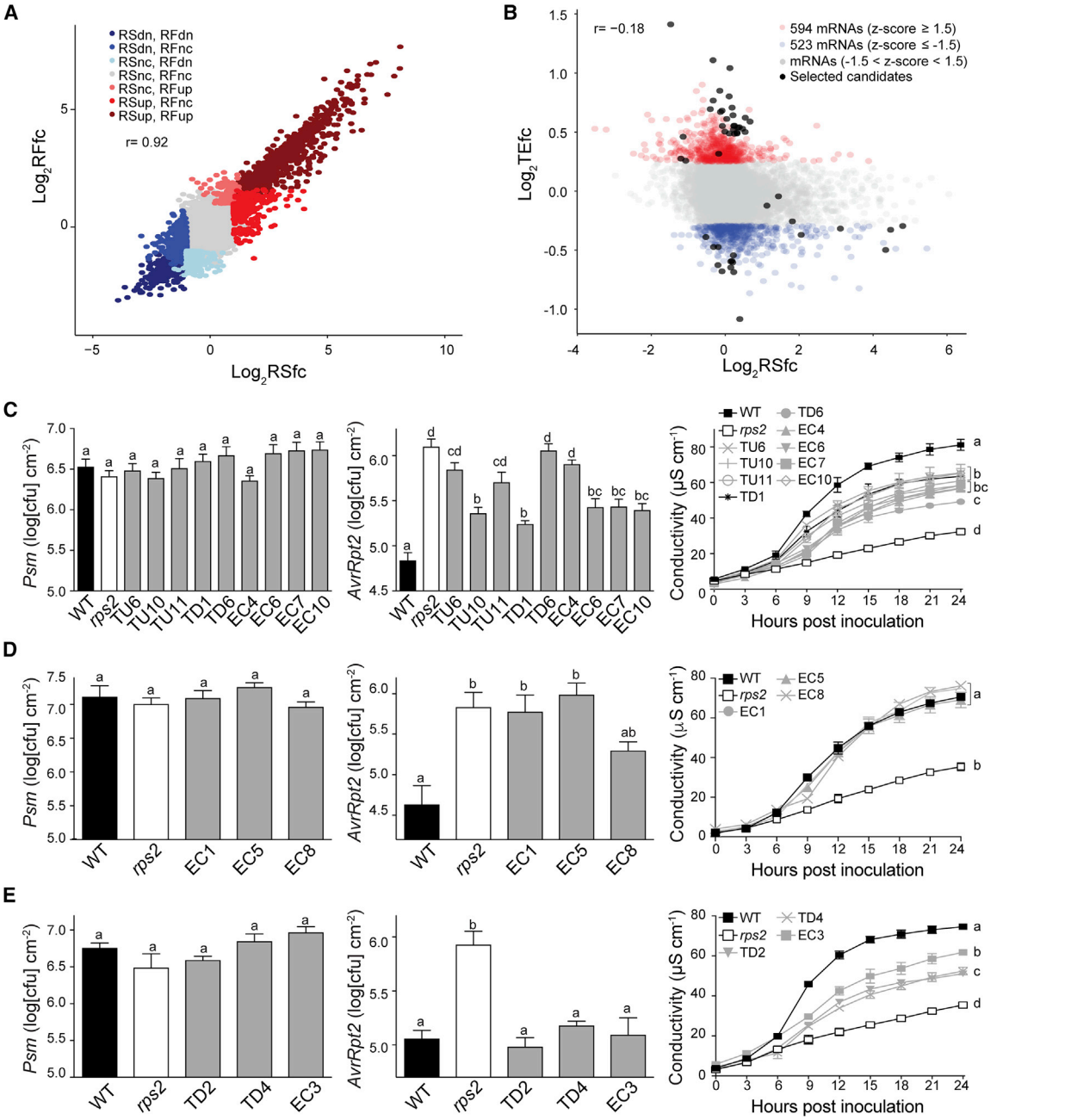

Figure 2. Identification of New Immune Regulators Based on Global Analysis of Translational Changes during RPS2-Mediated ETI.
(A and B) Relationships between RSfc and RFfc **(A)**, and between RSfc and TEfc **(B)** in WT. dn, down; nc, no change. Black dots, candidates selected for ETI phenotype testing.
(C–E) Growth of *Psm* ES4326 (left) or *Psm* ES4326/*AvrRpt2* (middle) (OD_{600nm} = 0.001), and ion leakage analysis (right) caused by *Psm* ES4326/*AvrRpt2* (OD_{600nm} = 0.01) in phenotypic group A **(C)**, group B **(D)**, and group C **(E)** of new immune regulators. WT and *rps2* were used as controls. TU, TEup; TD, TEdn; EC, ETI candidate. Different letters indicate values that are significantly different based on Tukey's test ($P < 0.01$; one-way ANOVA). For ion leakage analysis, the last time point was used for statistical analysis. Data are means ± SEM; $n = 8$ biological replicates for bacterial growth and $n = 3$ biological replicates for ion leakage analysis.

in the methodology. These data suggest that, even though translational induction is highly coordinated with transcriptional activation, translational regulation plays a significant role in regulating ETI. To dissect how much the transcriptional and translational components contribute to these individual candidates in defense, future study using mutants separating these processes will be required.

Phenotypes of these ETI-deficient mutants confirmed the involvement of sphingolipids in ETI (Berkey et al., 2012; Sánchez-Rangel et al., 2015) and suggested possible roles for ABA perception and amino acid transporters in the immune response beyond basal resistance (Lim and Lee, 2015; Yang et al., 2014). Another striking result of the mutant analysis is the involvement of additional receptors including TIR–NBS–LRRs, a

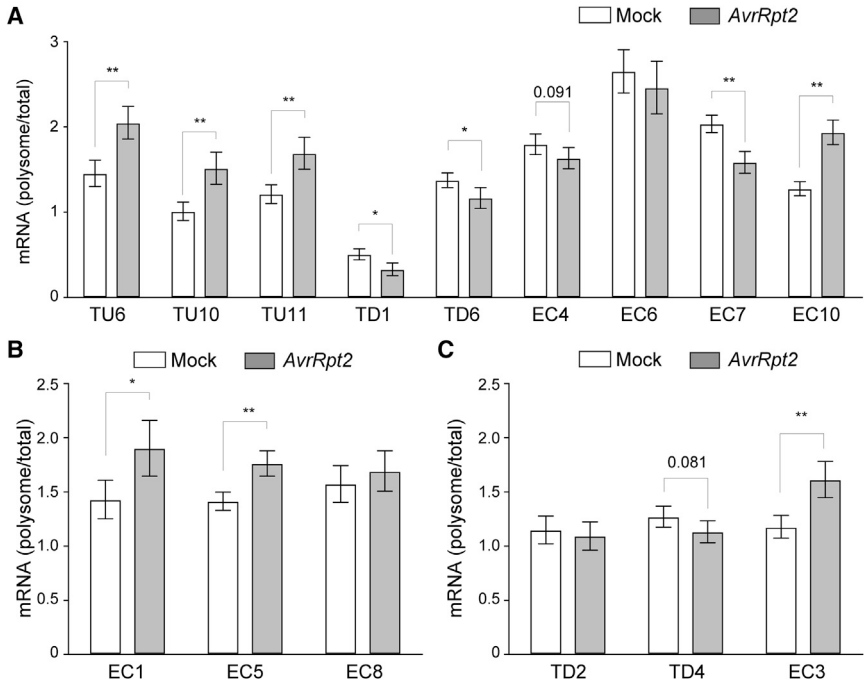

Figure 3. mRNA Association with Ribosomes upon ETI Induction.

(A–C) Ribosomal associations of ETI-gene mRNAs were calculated as polysomal/total mRNA fractions with mock or ETI (AvrRpt2) induction. Expression levels were normalized against *UBQ5*. **(A–C)** correspond to Figure 2C–2E, respectively. Data are means ± SD; $n = 3$ three biological replicates. Data were combined using linear mixed effect model (lme4) with experiment as random effects; $^{*}P < 0.05$, $^{**}P < 0.01$ as determined by Student's t test. See also Supplemental Table 1.

TIR–NBS, and an LRR in conferring AvrRpt2-induced resistance, which is known to be mediated by the coiled-coil NBS–LRR, RPS2. This result suggests that these additional proteins are likely "helper receptors" aiding in completion of RPS2 activation. Alternatively, these additional receptors may function downstream of RPS2 activation to establish full resistance (Bonardi et al., 2011). In contrast to the *rps2* mutant, single knockout mutants of these receptors only partially compromised RPS2-mediated ETI (EC6, EC7, EC8, and EC10; Figure 2C and 2D). How these helper receptors contribute to RPS2-mediated ETI, and whether they interact with RPS2 or its cellular target RIN4 (Belkhadir et al., 2004; Day et al., 2005) requires further investigation.

Translational Dynamics of Metabolic Pathway Genes during ETI

To broaden our investigation on the transcriptional and translational changes that occur during ETI, we performed gene ontology (GO) enrichment analysis (Katari et al., 2010) on the genes differentially regulated in either RS or RF (Supplemental Data 4) to highlight and compare the physiological pathways that were affected transcriptionally and/or translationally during ETI. In addition to the expected biotic stress response GO terms enriched in both RS and RF samples, we found GO terms associate with several metabolic pathways including "cellular aromatic compound metabolic process" and "indole-containing compound metabolism." Enrichment of these terms suggests that metabolic pathways involved in aromatic amino acid biosynthesis may be regulated during ETI. To further study ETI-associated metabolic dynamics, we focused on RS and RF changes for the genes involved in metabolic pathways linked to the aromatic amino acid biosynthesis, including glycolysis, the pentose phosphate pathway, as well as the phenylpropanoid and camalexin biosynthesis pathways (Figure 4 and Supplemental Table 2). Interestingly, in our previous PTI analysis (Xu et al., 2017a), fewer genes in those pathways showed changes in RS and RF (Supplemental Figure 4). To determine whether these changes are specific to aromatic amino acids or general to other amino acids as well, we analyzed RF changes for all the amino acid biosynthesis pathways. We found that although some fluxes were linked to certain amino acids, including alanine, methionine, and glutamine, translational induction was mostly associated with enzymes involved in aromatic amino acid biosynthetic pathways (Supplemental Figure 5 and Supplemental Table 3). These results suggest that induction of ETI may involve dynamic changes in plants' primary metabolism. We next examined the "cellular aromatic compound metabolic process" GO term enriched in RSup and RFup genes to identify possible differences in ETI-induced transcriptional and translational activities. We found that "phenylpropanoid metabolic process" is uniquely enriched in the RFup genes, but absent from the RSup genes (Supplemental Figure 6), suggesting that translational upregulation of this secondary metabolic pathway branched from the aromatic amino acid, phenylalanine, may be important for the induction of ETI.

Dynamics of Amino Acid Metabolism during ETI

To test the hypothesis that plants actively control amino acid biosynthesis as a defense mechanism during ETI, we first performed amino acid profiling at 8 hpi and found that several amino acids had either an increase or a decrease in their levels during ETI (Figure 5A). Among the three aromatic amino acids, phenylalanine level was significantly increased, while tyrosine and tryptophan levels were decreased. Interestingly, the reduction in tryptophan is contrary to the upregulation of genes within the tryptophan biosynthetic pathway (Figure 4). The observed decrease in the tryptophan level may be due to a potential increase in the biosynthesis of the tryptophan-derived antimicrobial phytoalexin, camalexin (Lemarié et al., 2015), through the dramatic increases in both RS and RF (66-fold) of the key camalexin biosynthetic enzyme, tryptophan N-monooxygenase, CYP79B2 (EC 1.14.14.156; Figure 4 and Supplemental Figure 7A). Moreover, the *CYP79B2* mRNA had a slight increase of ribosomal association upon ETI induction in the ribosome pelleting experiment, suggesting a potential contribution of translational regulation (Supplemental Figure 7B). Indeed, the *cyp79B2* mutant showed reduced PCD, indicating the importance of camalexin biosynthesis in this

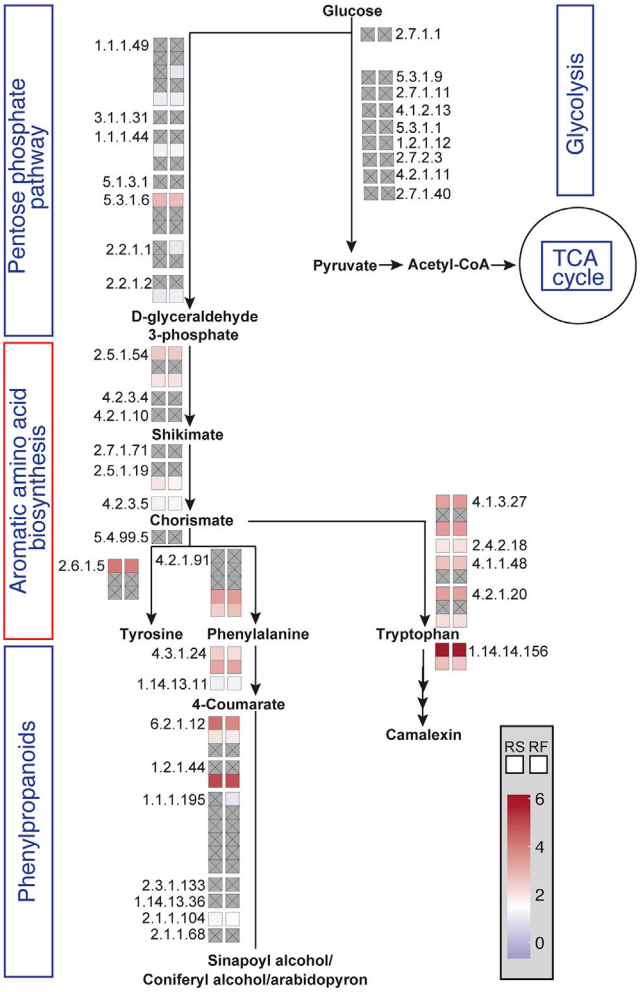

Figure 4. Transcriptional and Translational Dynamics of Specific Metabolic Pathways during ETI.

The schematic representation of metabolic pathways with each enzymatic step (EC number) generated using MetaCyc Metabolic Pathway Database (Caspi et al., 2018). The fold changes are shown with colors for transcription (left box) and translation (right box). Gray box with inscribed x indicates no significant change detected.

RPS2-mediated response (Supplemental Figure 7C). The increase in phenylalanine is consistent with the observed increase in both RS and RF of its biosynthesis genes (Figure 4). It is also consistent with the translational upregulation of genes within the phenylpropanoid pathway since phenylalanine is a precursor of phenylpropanoid biosynthesis, which has been associated with plant stress responses (Dixon and Paiva, 1995). The decreased tyrosine level during ETI might be associated with the phenylalanine increase, because tyrosine shares the upstream biosynthetic pathway with phenylalanine and is known to be the best amino donor for cytosolic phenylalanine biosynthesis (Yoo et al., 2013).

Contribution of Phenylalanine and Phenylalanine-Derived Phenylpropanoid Pathways to PCD and ETI

We next tested whether phenylalanine and its secondary metabolites in the phenylpropanoid pathway are important to confer ETI in plants. We examined genes in these metabolic pathways and found those encoding arogenate dehydratase 4 and 5 (ADT4 and ADT5, respectively) for phenylalanine synthesis (EC 4.2.1.91), and phenylalanine ammonia lyase 1 (PAL1) for conversion of phenylalanine to phenylpropanoid compounds were among the RF upregulated genes (EC 4.3.1.24; Figure 4 and Supplemental Table 2). The ribosome pelleting experiment confirmed the pattern of ETI-induced association with the ribosome for the *ADT5* mRNA (Figure 5B). The importance of PAL1 for plant immunity has been shown previously (Huang et al., 2010; Kim and Hwang, 2014), but its involvement in RPS2-mediated ETI is unknown.

To determine their roles in ETI, we obtained *adt4*, *adt5*, and *pal1* mutants and compared bacterial growth and PCD in these mutants with WT. We observed more bacterial growth specific to *Psm* ES4326/*AvrRpt2* that carries the effector in *adt4* and *adt5* than WT (Figure 5C), but with no significant difference in PCD (Figure 5D). In contrast, we observed a significant reduction in ETI-associated PCD in *pal1* without a clear increase in *Psm* ES4326/*AvrRpt2* growth (Figure 5C and 5D). These results support a positive role for phenylalanine and its secondary metabolites in ETI, both at the level of PCD regulation and at the level of immunity.

To eliminate possible direct effects of Phe or Phe derivatives on pathogen growth, we made use of lines carrying a dexamethasone (DEX)-inducible *AvrRpt2* transgene in WT and *rps2* backgrounds (Axtell et al., 2001). Induction of the bacterial effector *AvrRpt2* expression in the plants by DEX treatment can lead to PCD in an RPS2-dependent manner. We tested the effect of phenylalanine treatment 3 h before DEX induction and observed an increase in the level of ion leakage in the phenylalanine-treated plants compared with the control (Figure 5E). To complement increasing the level of phenylalanine through exogenous application, we also looked for a way to reduce the level of phenylalanine. Because it has been previously suggested that the pentose phosphate pathway contributes to the biosynthesis of aromatic amino acids (e.g., phenylalanine) by producing the aromatic amino acid precursor erythrose 4-phosphate (Khan, 2017), we hypothesized that inhibition of the pentose phosphate pathway will lead to a decrease in phenylalanine synthesis, and thus reduced PCD. To test this hypothesis, we treated plants with 6-aminonicotinamide (6AN), an inhibitor of glucose-6-phosphate dehydrogenase, the first enzyme of the pentose phosphate pathway, and found a significant reduction in AvrRpt2-mediated PCD (Figure 5F). Together, these results suggest that during ETI, both transcription and translation of metabolic enzymes contribute to increased levels of phenylalanine and its derivatives, which directly affect effector-triggered PCD and immunity.

DISCUSSION

Our study on global translational regulation during ETI establishes a link between immune response and metabolic dynamics. Global translational regulation during ETI is distinct from that during PTI, suggesting that plants operate complicated and dynamic translational mechanisms in response to specific immune stimuli. Unlike our PTI study (Xu et al., 2017a), a search for potential consensus in the 5′ leader sequences and 3′ UTRs did not yield any *cis* element in the mRNAs with ETI-mediated RF changes.

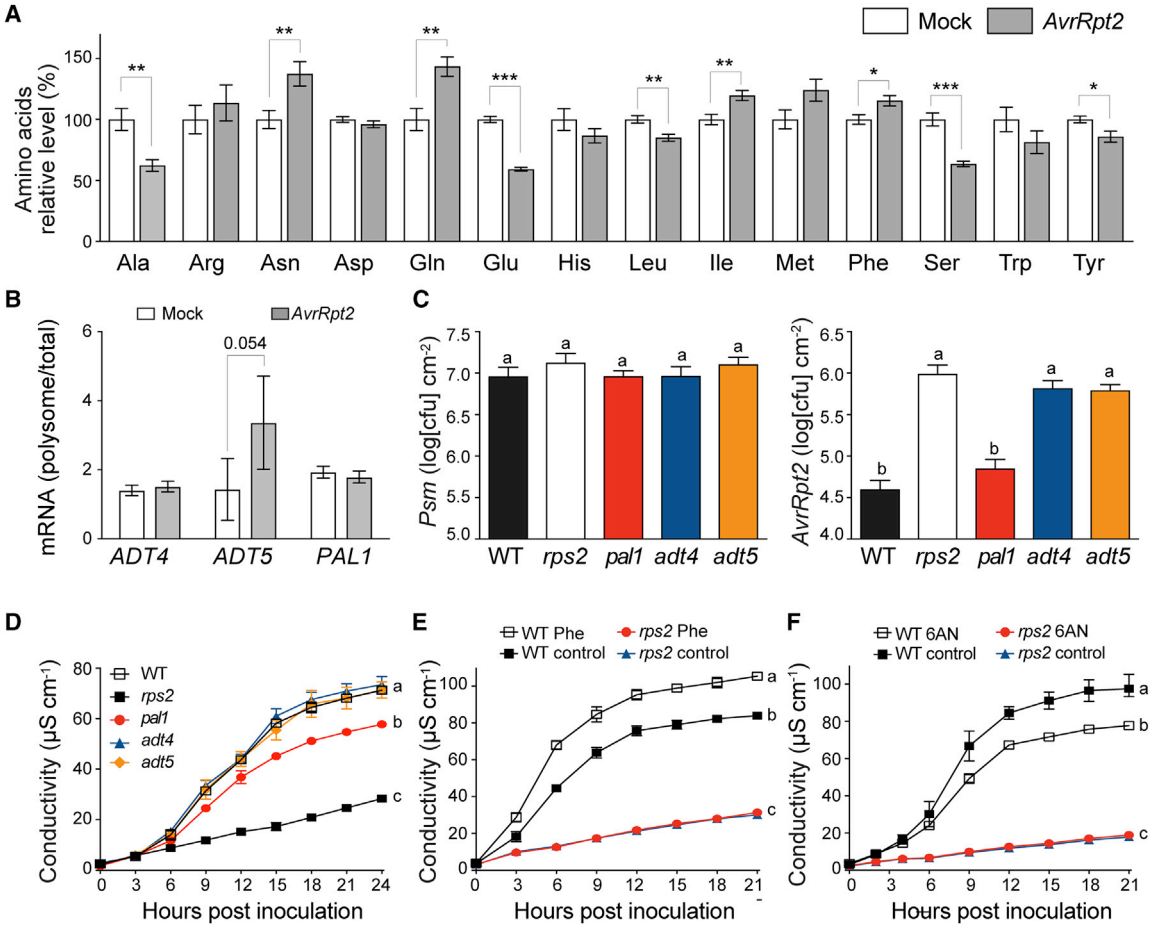

Figure 5. Phenylalanine and Its Derivatives Are Important for ETI Response.

(A) Levels of amino acids during ETI. Data are means ± SEM; *n* = 8 biological replicates from two experiments. **P* < 0.05, ***P* < 0.01, ****P* < 0.001 as determined by Student's *t* test (Met *P* = 0.063).

(B) Ribosomal associations of *ADT4*, *ADT5*, and *PAL1* mRNAs were calculated as polysomal/total RNA fractions with mock or ETI (AvrRpt2) induction. Expression levels were normalized against *UBQ5*. Data are means ± SD; *n* = 3 biological replicates. Data were combined using linear mixed effect model (lme4) with experiment as random effects and Student's *t* test was performed.

(C and D) Growth of *Psm* ES4326 (left) and *Psm* ES4326/*AvrRpt2* (right) **(C)**, and ion leakage caused by *Psm* ES4326/*AvrRpt2* **(D)** (OD_{600nm} = 0.001 for bacterial growth and 0.01 for ion leakage). Data are means ± SEM; *n* = 8 biological replicates for bacterial growth and *n* = 3 biological replicates for ion leakage analysis.

(E) Ion leakage analysis with exogeneous phenylalanine (Phe) treatment (5 mM) in WT and *rps2* plants. Data are means ± SEM; *n* = 4 biological replicates.

(F) Ion leakage analysis with exogenous 6-aminonicotinamide (6AN) treatment (1.25 mM) in WT and *rps2* plants. Data are means ± SEM; *n* = 3 biological replicates. **(C–F)** Different letters indicate values that are significantly different based on Tukey's test (*P* < 0.01; one-way ANOVA). For ion leakage analysis, the last time point was used for statistical analysis.

This suggests that the coordinated translational change upon ETI may be accomplished through modifications of the translational machinery instead of specific sequences in the mRNAs. Alternatively, such mRNA *cis*-elements might be difficult to capture due to the small number of genes with large TE changes.

We compared the AvrRpt2 response to previously reported translational regulation in response to *in planta* expression of a different effector molecule, AvrRpm1 (Meteignier et al., 2017) to determine whether the translational effect observed during ETI is specific for the individual effector molecule. We found that 50% of up- and 5% of downregulated genes from the RPS2-mediated transcriptional response overlapped with the RPM1-mediated transcriptional response, while 80% up- and 75% downregulated genes overlapped in the translational response (Figure 6 and Supplemental Data 5). This result suggests that, although AvrRpt2 and AvrRpm1 are recognized by different NBS–LRRs, there is not only a significant overlap in the downstream transcriptional events as reported previously (Mine et al., 2018), but also in translational activities as well. Recognition of AvrRpm1 by RPM1 also induced genes in metabolic pathways including "indole-containing compound metabolic process" and "aromatic amino acid family metabolic process" (Meteignier et al., 2017), suggesting that translational changes in metabolic pathways during ETI are likely a general pattern. Furthermore, 8 of the 11 TIR–NBS domain-containing genes and two of the three LRR genes in the RPS2-mediated response also showed significant changes in association with ribosomes after DEX-induced AvrRpm1 expression (Meteignier et al., 2017) (Supplemental Data 5). This result suggests that,

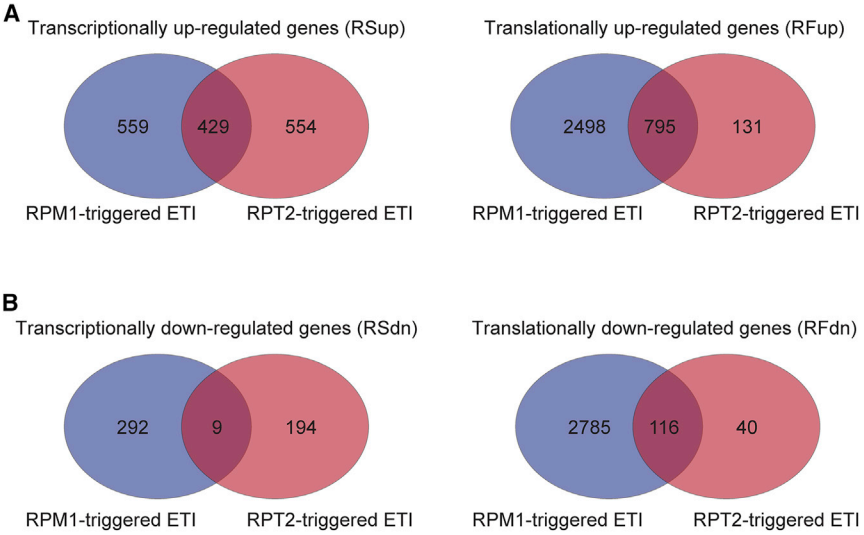

Figure 6. Venn Diagrams of Transcriptional and Translational Responses from the AvrRpm1 and AvrRpt2 Datasets.

(A) Venn diagrams showing numbers of overlapping and non-overlapping transcriptionally upregulated genes (RSup) and translationally upregulated genes (RFup) between the AvrRpm1 (blue) and AvrRpt2 (red) datasets.

(B) Venn diagrams showing numbers of overlapping and non-overlapping transcriptionally downregulated genes (RSdn) and translationally downregulated genes (RFdn) between the AvrRpm1 and AvrRpt2 datasets. RS, RNA-seq; RF, ribosomal footprinting; fc, fold change; up, upregulated; dn, downregulated.

beyond initial recognition of AvrRpm1 and AvrRpt2 by their cognate receptor RPM1 and RPS2, respectively, other helper receptors likely contribute to core ETI signaling. Future experiments are needed to test whether any of the commonly identified translationally regulated genes are also required for ETI mediated by RPM1.

Accumulating evidence suggests that amino acid metabolism plays an active role in plant immunity. Exogenous application of proline induced hypersensitive response-like cell death in *Arabidopsis* (Deuschle et al., 2004), whereas threonine has been shown to directly inhibit the growth of the oomycete pathogen *Hyaloperonospora arabidopsidis* (Stuttmann et al., 2011). Also, lysine-derived pipecolic acid has been reported as a key regulator of systemic acquired resistance (Návarová et al., 2012; Hartmann et al., 2018). Our study not only discovered that phenylalanine is important for ETI, but also establishes that translational regulation is a key regulatory mechanism of phenylalanine biosynthetic pathways during ETI. Furthermore, through our global translatome analysis, we discovered novel regulators and metabolic pathways involved in RPS2-mediated ETI. Although these metabolic pathways have been suggested to play a role in plant defense by many studies based on cDNA array, RNA-seq, and/or metabolic profiling (Scheideler et al., 2002; Ward et al., 2010; Aliferis et al., 2014; Misra et al., 2016; Schwachtje et al., 2018), our discovery provides a strong piece of evidence that plants actively control biosynthetic pathways for phenylalanine and phenylalanine-derived compounds at both transcriptional and translational levels to activate the ETI defense program.

METHODS

Plant Materials and Growth Conditions

Plants were grown on soil (Metro Mix 360) at 22°C under a 12/12-h light/dark cycle with 55% humidity. The *Arabidopsis* transgenic lines carrying the *35S:uORFs$_{TBF1}$-LUC* construct in WT background was described previously (Xu et al., 2017a) and in *rps2* background was generated by genetic crossing. *adt4* (SALK_065483), *adt5* (SALK_088171), *pal1* (SALK_000357), and *cyp79B2* (SALK_113348), and other T-DNA insertion mutants used in this study were obtained from the Arabidopsis Biological Resource Center (Supplemental Data 3 and Supplemental Data 6).

LUC Activity Measurement

To record the *35S:uORFs$_{TBF1}$-LUC* reporter activity, 4-week-old transgenic plants were sprayed with 1 mM luciferin (Gold Biotechnology) 12 h before infiltration with either *Psm* ES4326/*AvrRpt2* (OD_{600nm} = 0.02) or 10 mM $MgCl_2$. Luciferase activity was recorded in a CCD camera-equipped box (Nightshade Company) with each exposure time of 20 min.

Ribosome Pelleting and Ribo-Seq Library Construction

Ribo-seq libraries were constructed as described previously (Ingolia et al., 2012; Xu et al., 2017a). In brief, leaves (0.3 g) from 4-week-old transgenic plants were collected, ground in liquid nitrogen, and resuspended in 2 ml of pre-chilled polysome extraction buffer (PEB). Ribosomes were purified using a sucrose cushion after ultra-centrifugation at 4°C (70 000 rpm for 4 h). For the ribosome pelleting experiment, the samples were washed twice with cold water and resuspended in TRIzol (Ambion) to extract ribosome-associated mRNA. For Ribo-seq library construction, the pellet was washed twice with cold water and resuspended in 300 μl of RNase I digestion buffer. The supernatant was then transferred to new tubes and incubated with 10 μl of RNase I (100 U μl^{-1}) at 25°C for 60 min. Then, 15 μl of SUPERase-In (20 U μl^{-1}) was added to halt the reaction. Subsequent steps of library construction were performed as previously reported (Figure 1A; Ingolia et al., 2012; Xu et al., 2017a).

RNA-Seq Library Construction

RNA-seq library was constructed as described previously (Xu et al., 2017a). In brief, 0.75 ml TRIzol LS (Ambion) was added to the 0.25 ml lysate saved from the Ribo-seq library construction. Total RNA was extracted, quantified and qualified using NanoDrop (Thermo Fisher Scientific). Total RNA (50–75 μg) was used for mRNA purification with Dynabeads Oligo $(dT)_{25}$ (Invitrogen). Purified poly(A) mRNA (20 μl) was mixed with 20 μl of 2× fragmentation buffer (2 mM EDTA, 10 mM Na_2CO_3, 90 mM $NaHCO_3$) and incubated at 95°C for 40 min before cooling on ice. Cold water (500 μl), 1.5 μl of GlycoBlue, and 60 μl of cold 3 M sodium acetate were then added to the samples and mixed. Subsequently, 600 μl of isopropanol was added and incubated at –80°C for at least 30 min to precipitate RNA. Samples were then centrifuged at 4°C (12 000 rpm for 30 min) to remove all liquid and air-dried for 10 min before resuspension in 5 μl of 10 mM Tris (pH 8.0). Remaining steps were performed equivalently to the Ribo-seq library preparation.

Quality Check of Ribo-Seq and RNA-Seq

Library quality was validated using a bioanalyzer profile, which detected the expected peak at ~176 bp. In the RF samples, we detected a peak length distribution at 30 nt, consistent with the expected length protected

by a ribosome, but no specific peak in the RS data (Supplemental Figures 1A and 2A). RF coverage was the highest at the translation initiation codon and showed a preference for reads in the first frame (Supplemental Figures 1B, 1C, 2B, and 2C). Detected coverage of ribosome footprints in the 5′ leader sequence and 3′ UTR is affected by digestion buffer conditions (Hsu et al., 2016). Reads in 5′ leader sequence and 3′ UTR could occur under buffer conditions allowing the capture of ribosomes in different conformations, in mature plants, and in response stress. Moreover, there is a possibility that other RNA-binding proteins interacting with 5′ leader sequences and 3′ UTRs under certain circumstance as described previously (Dunn et al., 2013; Miettinen and Björklund, 2015). Hierarchical clustering and Pearson correlation of expression showed strong reproducibility among replicates with the same treatment for each genotype (Supplemental Figures 1D, 1E, 2D, and 2E), and the range of RFfc and RSfc appeared to be similar (Supplemental Figures 1F and 2F). Strong correlations between mRNA abundance (RS) and ribosome association (RF) were detected within the same treatment (i.e., Mock or AvrRpt2) for WT (Supplemental Figure 1G) and *rps2* plants (Supplemental Figure 2G).

Polysome Profiling

Polysome profiling was performed as reported previously (Xu et al., 2017a). In brief, 0.5 g of 4-week-old leaves was ground in liquid nitrogen and resuspended in 2 ml of pre-chilled PEB buffer. Crude lysate (1 ml) was loaded to a sucrose gradient (15%–60%) and centrifuged at 4°C (35 000 rpm for 10 h). Polysome-associated mRNA was isolated through fractionation using a sucrose gradient.

Psm ES4326/*AvrRpt2* Bacterial Growth and Ion Leakage Measurement

For bacterial growth assays, 4-week-old plants were infiltrated with *Psm* ES4326/*AvrRpt2* or *Psm* ES4326 (OD_{600nm} = 0.001). Infected and mock-infiltrated leaves were collected 3 days post infiltration. Leaf discs were ground in solution containing 10 mM $MgCl_2$ and plated in dilution series onto plates containing King's B medium (KB) supplemented with 100 μg ml^{-1} streptomycin and 10 μg ml^{-1} tetracycline for *Psm* ES4326/*AvrRpt2* or KB with 100 μg ml^{-1} streptomycin for *Psm* ES4326. Bacterial growth was scored 3 days after plating. For ion leakage measurement, plants were infiltrated with *Psm* ES4326/*AvrRpt2* (OD_{600nm} = 0.01). After 1 h, leaf discs were collected from infiltrated leaves and ion leakage was measured every 3 h for 24 h using the conductivity meter (Thermo Scientific).

Chemical Applications

6AN (1.25 mM; Sigma-Aldrich) dissolved in 1.25% DMSO or mock (1.25% DMSO only) was sprayed 1 day before 50 μM DEX induction. L-phenylalanine (5 mM) (Sigma-Aldrich) or mock (water only) was sprayed 3 h before DEX spray. Leaf discs were collected from infiltrated leaves 1 h after DEX induction and ion leakage was measured every 3 h for 21–24 h.

Quantitative Real-Time RT–PCR

Total RNA was extracted from approximately 50 mg of leaf tissue using TRIzol (Ambion) based on manufacturer's instruction. After DNase I (Ambion) treatment, cDNA synthesis was performed by the instruction of SuperScript III Reverse Transcriptase (Invitrogen) using oligo(dT). Quantitative real-time RT–PCR was performed with FastStart Universal SYBR Green Master (Roche). For polysome profiling, mRNA was extracted from each fraction while total mRNA was extracted from the crude lysate. Expression level in each fraction was normalized to total mRNA abundance.

Amino Acid Profiling and High-Performance Liquid Chromatography Analysis

Approximately 0.2 g of leaves from 4-week-old plants were collected, ground in liquid nitrogen, and resuspended in 0.8 ml of extraction buffer containing 2-amino-2-methyl-1-propanol hydrochloride (Sigma) in 75% ethanol (pH was adjusted to pH 10 by NaOH). As an internal standard, 60 nmol aminoadipic acid (Sigma-Aldrich) was added into the extraction buffer. The extract was centrifuged at 4°C (12 000 rpm for 30 min). Supernatant was collected and filtered through a 10-kDa MWCO Amicon column (EMD-Millipore) by centrifugation at 4°C (3500 rpm for 90 min). The filtered solution was dried with SpeedVac (45°C for 3 h; Eppendorf), and the pellet was stored at –20°C for 30 min and dissolved in 50 μl of water. The final reaction mixture (10 μl) was derivatized with o-phthalaldehyde (Agilent) and analyzed on the Agilent 1100 high-performance liquid chromatography system using the ZORBAX Eclipse AAA column (3.5 μm, 3.0 × 140 mm; Agilent) at a flow rate of 0.45 ml min^{-1} with a 40-min linear gradient of 0%–30% methanol and acetone in 15 mM ammonium acetate bufferpH 7.8.

Bioinformatic and Statistical Analyses

Bioinformatic and statistical analyses were performed as described previously (Xu et al., 2017a). In brief, Bowtie2 was used to align reads to the *Arabidopsis* TAIR10 genome (Langmead and Salzberg, 2012). Read assignment to genes was achieved using high-throughput sequencing (Anders et al., 2015) for transcriptome and translatome libraries by exon and CDS, respectively. Transcriptome and translatome fold changes (i.e., RSfc and RFfc) were calculated using DESeq2 (Love et al., 2014). TE was calculated by combining reads for all genes that passed reads per kilobase of transcript per million mapped reads (RPKM) $\geq$1 in CDS threshold in all biological replicates and normalizing Ribo-seq RPKM to RNA-seq RPKM as reported. Density plot was presented using IGB (Nicol et al., 2009). Statistical analysis was done by one-way ANOVA with Tukey's honest significant difference test for Figures 1B, 2C–2E, 5C–5F, and Supplemental Figure 7C. Statistical analysis was done using Student's *t*-test for Figure 5A. GraphPad Prism six was used for all the statistical analyses. For qPCR data (Figure 1B and 1D), *n* indicates technical repeats, which were verified by two or three independent experiments. All other replicates indicate biological replicates.

The RS and RF data presented in this publication have been deposited in NCBI's GEO (GEO: GSE124115).

SUPPLEMENTAL INFORMATION

Supplemental Information is available at *Molecular Plant Online*.

FUNDING

This study was supported by grants from NIH R35GM118036-02, NSF IOS 1645589, and HHMI-GBMF (grant no. GBMF3032) to X.D. and a Hargitt fellowship to H.Y.

AUTHOR CONTRIBUTIONS

H.Y., G.X., and X.D. designed the research. H.Y., G.X., and J.M. optimized the Ribo-seq protocol. H.Y. and M.Y. performed qPCR experiments. H.Y., M.Y., and D.B. performed ion leakage and bacterial growth experiments. G.X. and L.L. generated the reporter lines. H.Y. performed the rest of the experiments. G.H.G. performed all the bioinformatic analyses. All authors analyzed the data. H.Y. and X.D. wrote the manuscript with the input from all authors.

ACKNOWLEDGMENTS

We thank George Dubay for assisting with the amino acid analysis, Jenny Shen for helping with the MetaCyc analysis, Musoki Mwimba for linear modeling of ribosome pelleting experiments, and Paul J. Zwack, Sophia G. Zebell, and Dong lab members for critical comments on this project. No conflict of interest is declared.

Received: August 9, 2019
Revised: September 9, 2019
Accepted: September 16, 2019
Published: September 27, 2019

REFERENCES

Aboul-Soud, M.A., Chen, X., Kang, J.G., Yun, B.W., Raja, M.U., Malik, S.I., and Loake, G.J. (2009). Activation tagging of ADR2 conveys a spreading lesion phenotype and resistance to biotrophic pathogens. New Phytol. **183**:1163–1175.

Aliferis, K.A., Faubert, D., and Jabaji, S. (2014). A metabolic profiling strategy for the dissection of plant defense against fungal pathogens. PLoS One **9**:e111930.

Anders, S., Pyl, P.T., and Huber, W. (2015). HTSeq—a Python framework to work with high-throughput sequencing data. Bioinformatics **31**:166–169.

Aravind, L., and Koonin, E.V. (1999). G-patch: a new conserved domain in eukaryotic RNA-processing proteins and type D retroviral polyproteins. Trends Biochem. Sci. **24**:342–344.

Axtell, M.J., McNellis, T.W., Mudgett, M.B., Hsu, C.S., and Staskawicz, B.J. (2001). Mutational analysis of the *Arabidopsis RPS2* disease resistance gene and the corresponding *Pseudomonas syringae avrRpt2* avirulence gene. Mol. Plant Microbe Interact. **14**:181–188.

Belkhadir, Y., Nimchuk, Z., Hubert, D.A., Mackey, D., and Dangl, J.L. (2004). *Arabidopsis* RIN4 negatively regulates disease resistance mediated by RPS2 and RPM1 downstream or independent of the NDR1 signal modulator and is not required for the virulence functions of bacterial type III effectors AvrRpt2 or AvrRpm1. Plant Cell **16**:2822–2835.

Berkey, R., Bendigeri, D., and Xiao, S. (2012). Sphingolipids and plant defense/disease: the ''death'' connection and beyond. Front. Plant Sci. **3**:68.

Bonardi, V., Tang, S., Stallmann, A., Roberts, M., Cherkis, K., and Dangl, J.L. (2011). Expanded functions for a family of plant intracellular immune receptors beyond specific recognition of pathogen effectors. Proc. Natl. Acad. Sci. U S A **108**:16463–16468.

Caspi, R., Billington, R., Fulcher, C.A., Keseler, I.M., Kothari, A., Krummenacker, M., Latendresse, M., Midford, P.E., Ong, Q., Ong, W.K., et al. (2018). The MetaCyc database of metabolic pathways and enzymes. Nucleic Acids Res. **46**:D633–D639.

Coll, N.S., Vercammen, D., Smidler, A., Clover, C., Van Breusegem, F., Dangl, J.L., and Epple, P. (2010). *Arabidopsis* type I metacaspases control cell death. Science **330**:1393–1397.

Day, B., Dahlbeck, D., Huang, J., Chisholm, S.T., Li, D., and Staskawicz, B.J. (2005). Molecular basis for the RIN4 negative regulation of RPS2 disease resistance. Plant Cell **17**:1292–1305.

Deuschle, K., Funck, D., Forlani, G., Stransky, H., Biehl, A., Leister, D., van der Graaff, E., Kunze, R., and Frommer, W.B. (2004). The role of Δ^1-pyrroline-5-carboxylate dehydrogenase in proline degradation. Plant Cell **16**:3413–3425.

Dixon, R.A., and Paiva, N.L. (1995). Stress-induced phenylpropanoid metabolism. Plant Cell **7**:1085–1097.

Dunn, J.G., Foo, C.K., Belletier, N.G., Gavis, E.R., and Weissman, J.S. (2013). Ribosome profiling reveals pervasive and regulated stop codon readthrough in *Drosophila melanogaster*. Elife **2**:e01179.

Grant, M.R., Godiard, L., Straube, E., Ashfield, T., Lewald, J., Sattler, A., Innes, R.W., and Dangl, J.L. (1995). Structure of the *Arabidopsis* RPM1 gene enabling dual specificity disease resistance. Science **269**:843–846.

Gu, Y., Zebell, S.G., Liang, Z., Wang, S., Kang, B.H., and Dong, X. (2016). Nuclear pore permeabilization is a convergent signaling event in effector-triggered immunity. Cell **166**:1526–1538.

Hartmann, M., Zeier, T., Bernsdorff, F., Reichel-Deland, V., Kim, D., Hohmann, M., Scholten, N., Schuck, S., Bräutigam, A., Hölzel, T., et al. (2018). Flavin monooxygenase-generated N-hydroxypipecolic acid is a critical element of plant systemic immunity. Cell **173**:456–469.

Hsu, P.Y., Calviello, L., Wu, H.L., Li, F.W., Rothfels, C.J., Ohler, U., and Benfey, P.N. (2016). Super-resolution ribosome profiling reveals unannotated translation events in *Arabidopsis*. Proc. Natl. Acad. Sci. U S A **113**:E7126–E7135.

Huang, J., Gu, M., Lai, Z., Fan, B., Shi, K., Zhou, Y.H., Yu, J.Q., and Chen, Z. (2010). Functional analysis of the *Arabidopsis PAL* gene family in plant growth, development, and response to environmental stress. Plant Physiol. **153**:1526–1538.

Ingolia, N.T., Brar, G.A., Rouskin, S., McGeachy, A.M., and Weissman, J.S. (2012). The ribosome profiling strategy for monitoring translation *in vivo* by deep sequencing of ribosome-protected mRNA fragments. Nat. Protoc. **7**:1534–1550.

Ingolia, N.T., Ghaemmaghami, S., Newman, J.R., and Weissman, J.S. (2009). Genome-wide analysis *in vivo* of translation with nucleotide resolution using ribosome profiling. Science **324**:218–223.

Juntawong, P., Girke, T., Bazin, J., and Bailey-Serres, J. (2014). Translational dynamics revealed by genome-wide profiling of ribosome footprints in *Arabidopsis*. Proc. Natl. Acad. Sci. U S A **111**:E203–E212.

Katari, M.S., Nowicki, S.D., Aceituno, F.F., Nero, D., Kelfer, J., Thompson, L.P., Cabello, J.M., Davidson, R.S., Goldberg, A.P., Shasha, D.E., et al. (2010). VirtualPlant: a software platform to support systems biology research. Plant Physiol. **152**:500–515.

Khan, A.S. (2017). Flowering Plants: Structure and Industrial Products (Hoboken, NJ: John Wiley).

Kim, D.S., and Hwang, B.K. (2014). An important role of the pepper phenylalanine ammonia-lyase gene (*PAL1*) in salicylic acid-dependent signalling of the defence response to microbial pathogens. J. Exp. Bot. **65**:2295–2306.

Langmead, B., and Salzberg, S.L. (2012). Fast gapped-read alignment with Bowtie 2. Nat. Methods **9**:357–359.

Lei, L., Shi, J., Chen, J., Zhang, M., Sun, S., Xie, S., Li, X., Zeng, B., Peng, L., Hauck, A., et al. (2015). Ribosome profiling reveals dynamic translational landscape in maize seedlings under drought stress. Plant J. **84**:1206–1218.

Lemarié, S., Robert-Seilaniantz, A., Lariagon, C., Lemoine, J., Marnet, N., Levrel, A., Jubault, M., Manzanares-Dauleux, M.J., and Gravot, A. (2015). Camalexin contributes to the partial resistance of *Arabidopsis thaliana* to the biotrophic soilborne protist *Plasmodiophora brassicae*. Front. Plant Sci. **6**:539.

Lim, C.W., and Lee, S.C. (2015). *Arabidopsis* abscisic acid receptors play an important role in disease resistance. Plant Mol. Biol. **88**:313–324.

Liu, M.J., Wu, S.H., Wu, J.F., Lin, W.D., Wu, Y.C., Tsai, T.Y., Tsai, H.L., and Wu, S.H. (2013). Translational landscape of photomorphogenic *Arabidopsis*. Plant Cell **25**:3699–3710.

Love, M.I., Huber, W., and Anders, S. (2014). Moderated estimation of fold change and dispersion for RNA-seq data with DESeq2. Genome Biol. **15**:550.

Merchante, C., Brumos, J., Yun, J., Hu, Q., Spencer, K.R., Enríquez, P., Binder, B.M., Heber, S., Stepanova, A.N., and Alonso, J.M. (2015). Gene-specific translation regulation mediated by the hormone-signaling molecule EIN2. Cell **163**:684–697.

Meteignier, L.V., El Oirdi, M., Cohen, M., Barff, T., Matteau, D., Lucier, J.F., Rodrigue, S., Jacques, P.E., Yoshioka, K., and Moffett, P. (2017). Translatome analysis of an NB-LRR immune response identifies important contributors to plant immunity in *Arabidopsis*. J. Exp. Bot. **68**:2333–2344.

Miettinen, T.P., and Björklund, M. (2015). Modified ribosome profiling reveals high abundance of ribosome protected mRNA fragments derived from 3' untranslated regions. Nucleic Acids Res. **43**:1019–1034.

Mindrinos, M., Katagiri, F., Yu, G.L., and Ausubel, F.M. (1994). The *A. thaliana* disease resistance gene RPS2 encodes a protein containing a nucleotide-binding site and leucine-rich repeats. Cell **78**:1089–1099.

Mine, A., Seyfferth, C., Kracher, B., Berens, M.L., Becker, D., and Tsuda, K. (2018). The defense phytohormone signaling network enables rapid, high-amplitude transcriptional reprogramming during effector-triggered immunity. Plant Cell **30**:1199–1219.

Misra, B.B., de Armas, E., and Chen, S. (2016). Differential metabolomic responses of PAMP-triggered immunity and effector-triggered immunity in *Arabidopsis* suspension cells. Metabolomics **12**:61.

Návarová, H., Bernsdorff, F., Döring, A.C., and Zeier, J. (2012). Pipecolic acid, an endogenous mediator of defense amplification and priming, is a critical regulator of inducible plant immunity. Plant Cell **24**:5123–5141.

Nandety, R.S., Caplan, J.L., Cavanaugh, K., Perroud, B., Wroblewski, T., Michelmore, R.W., and Meyers, B.C. (2013). The role of TIR-NBS and TIR-X proteins in plant basal defense responses. Plant Physiol. **162**:1459–1472.

Nicol, J.W., Helt, G.A., Blanchard, S.G., Raja, A., and Loraine, A.E. (2009). The Integrated Genome Browser: free software for distribution and exploration of genome-scale datasets. Bioinformatics **25**:2730–2731.

Padmanabhan, M., Cournoyer, P., and Dinesh-Kumar, S.P. (2009). The leucine-rich repeat domain in plant innate immunity: a wealth of possibilities. Cell Microbiol. **11**:191–198.

Sánchez-Rangel, D., Rivas-San Vicente, M., de la Torre-Hernández, M.E., Nájera-Martínez, M., and Plasencia, J. (2015). Deciphering the link between salicylic acid signaling and sphingolipid metabolism. Front. Plant Sci. **6**:125.

Scheideler, M., Schlaich, N.L., Fellenberg, K., Beissbarth, T., Hauser, N.C., Vingron, M., Slusarenko, A.J., and Hoheisel, J.D. (2002). Monitoring the switch from housekeeping to pathogen defense metabolism in *Arabidopsis thaliana* using cDNA arrays. J. Biol. Chem. **277**:10555–10561.

Schwachtje, J., Fischer, A., Erban, A., and Kopka, J. (2018). Primed primary metabolism in systemic leaves: a functional systems analysis. Sci. Rep. **8**:216.

Stuttmann, J., Hubberten, H.M., Rietz, S., Kaur, J., Muskett, P., Guerois, R., Bednarek, P., Hoefgen, R., and Parker, J.E. (2011). Perturbation of *Arabidopsis* amino acid metabolism causes incompatibility with the adapted biotrophic pathogen *Hyaloperonospora arabidopsidis*. Plant Cell **23**:2788–2803.

Swiderski, M.R., Birker, D., and Jones, J.D. (2009). The TIR domain of TIR-NB-LRR resistance proteins is a signaling domain involved in cell death induction. Mol. Plant Microbe Interact. **22**:157–165.

Ward, J.L., Forcat, S., Beckmann, M., Bennet, M., Miller, S.J., Baker, J.M., Hawkins, N.D., Vermeer, C.P., Lu, C., Lin, W., et al. (2010). The metabolic transition during disease following infection of *Arabidopsis thaliana* by *Pseudomonas syringae* pv. *tomato*. Plant J. **63**:443–457.

Xu, G., Greene, G.H., Yoo, H., Liu, L., Marqués, J., Motley, J., and Dong, X. (2017a). Global translational reprogramming is a fundamental layer of immune regulation in plants. Nature **25**:487–490.

Xu, G., Yuan, M., Ai, C., Liu, L., Zhuang, E., Karapetyan, S., Wang, S., and Dong, X. (2017b). uORF-mediated translation allows engineered plant disease resistance without fitness costs. Nature **545**:491–494.

Yángüez, E., Castro-Sanz, A.B., Fernández-Bautista, N., Oliveros, J.C., and Castellano, M.M. (2013). Analysis of genome-wide changes in the translatome of *Arabidopsis* seedlings subjected to heat stress. PLoS One **8**:e71425.

Yang, H., Postel, S., Kemmerling, B., and Ludewig, U. (2014). Altered growth and improved resistance of *Arabidopsis* against *Pseudomonas syringae* by overexpression of the basic amino acid transporter AtCAT1. Plant Cell Environ **37**:1404–1414.

Yoo, H., Widhalm, J.R., Qian, Y., Maeda, H., Cooper, B.R., Jannasch, A.S., Gonda, I., Lewinsohn, E., Rhodes, D., and Dudareva, N. (2013). An alternative pathway contributes to phenylalanine biosynthesis in plants via a cytosolic tyrosine: phenylpyruvate aminotransferase. Nat. Commun. **4**:2833.

Zhang, Y., Yang, Y., Fang, B., Gannon, P., Ding, P., Li, X., and Zhang, Y. (2010). *Arabidopsis snc2-1D* activates receptor-like protein-mediated immunity transduced through WRKY70. Plant Cell **22**:3153–3163.